Microscopic signatures of yielding in concentrated nanoemulsions under large-amplitude oscillatory shear

Michael C. Rogers, Kui Chen, Matthew J. Pagenkopp, Thomas G. Mason, Suresh Narayanan, James L. Harden, and Robert L. Leheny

Phys. Rev. Materials **2**, 095601 — Published 10 September 2018

DOI: 10.1103/PhysRevMaterials.2.095601

Microscopic signatures of yielding in concentrated nanoemulsions under large-amplitude oscillatory shear

Michael C. Rogers,[1] Kui Chen,[2] Matthew J. Pagenkopp,[3] Thomas G. Mason,[3,4] Suresh Narayanan,[5] James L. Harden,[1,*] and Robert L. Leheny[2,†]

[1]*Department of Physics, University of Ottawa, Ottawa, Ontario, K1N 6N5, Canada*

[2]*Department of Physics and Astronomy, Johns Hopkins University, Baltimore, Maryland 21218, USA*

[3]*Department of Chemistry and Biochemistry, University of California-Los Angeles, Los Angeles, California 90095, USA*

[4]*Department of Physics and Astronomy, University of California-Los Angeles, Los Angeles, California 90095, USA*

[5]*X-Ray Science Division, Argonne National Laboratory, Argonne, Illinois 60439, USA*

(Dated: August 3, 2018)

Abstract

We report x-ray photon correlation spectroscopy (XPCS) experiments on a series of concentrated oil-in-water nanoemulsions with varying droplet volume fraction subjected to *in situ* steady-state large-amplitude oscillatory shear (LAOS). The shear strain causes periodic echoes in the x-ray speckle patterns that lead to peaks in the intensity autocorrelation function. Above an onset strain amplitude that depends on nanoemulsion concentration, the peaks become attenuated, signaling spatially heterogeneous, shear-induced droplet dynamics. These dynamics include irreversible re-arrangements among the droplets that occur in some regions of the nanoemulsions during a given shear cycle and residual strain-like displacements in those regions that do not re-arrange. The wave-vector dependence of the peak attenuation indicates a power-law distribution in the size of regions undergoing shear-induced rearrangement that is similar to that observed previously in LAOS-XPCS measurements on concentrated nanocolloidal gels. The values of the onset strains for re-arrangement correlate with the concentration-dependent macroscopic yielding behavior of the nanoemulsions. Specifically, they occur below the strains at which the nanoemulsions become effectively fluidized and, except for the lowest concentration nanoemulsion in the study, significantly above the threshold strain for nonlinear rheological response.

I. INTRODUCTION

Emulsions are part of a broad class of multiphase colloidal dispersions. Oil-in-water nanoemulsions consist of nanoscale oil droplets dispersed in water along with surfactant to prevent droplet coalescence. At low droplet volume fractions ϕ, the droplets freely diffuse, and the nanoemulsions are viscous fluids. At high ϕ, the droplets can become jammed in an arrested amorphous packing. Such concentrated nanoemulsions possess viscoelastic properties in which they display an elastic limit beyond which applied stress causes yielding[1]. While conventional rheological measurements can characterize the bulk mechanical signatures of yielding, they give no direct information about the droplet rearrangements that underlie yielding. Such experimental information connecting microscopic structural dynamics and macroscopic mechanical deformation is crucial to understanding the process of yielding[2] and particularly its dependence on ϕ. In this paper we address this need by using *in situ* x-ray speckle measurements to characterize shear-induced droplet dynamics that occur under large amplitude oscillatory shear (LAOS) in a set of concentrated nanoemulsions.

Stress-driven and flow-driven modifications of soft material microstructure have been investigated extensively using *in situ* x-ray and neutron scattering[3–19]. The associated microstructural dynamics, however, are less well studied experimentally[20–23]. Such dynamics have been measured in concentrated emulsions with micrometer-sized droplets under LAOS using diffusing wave spectroscopy (DWS)[21]. In this study, peaks in the time autocorrelation of the intensity of scattered coherent visible light were used to determine the fraction of irreversibly displaced droplets during cycles of the oscillatory shear. The multiple scattering intrinsic in DWS rendered the technique sensitive to motion over effectively a single length, and hence length-scale dependence of droplet rearrangements was inaccessible using this measurement technique. Different than DWS-LAOS experiments, Huang and Mason used time-resolved 2D-array detected angle-dependent laser light scattering to probe irreversible changes in the structure of concentrated emulsions of microscale droplets during and after imposed LAOS flows, revealing memory effects and differing degrees of disorder and order in droplet structures[24,25]. Microscopy has also been employed to track droplet motion in emulsions of micrometer-scale droplets under LAOS. In one such experiment, Clara-Rohala *et al.* observed how large polydispersity in emulsions can promote non-affine droplet displacements[26], while in another experiment Knowlton *et al.* tracked the shear-

induced heterogeneous dynamics and rapid increase in irreversible droplet displacements associated with rheological yielding[27].

While these studies have provided insight into the microscopic dynamics underlying deformation and yielding of emulsions composed of micrometer-scale droplets, the relevance of their findings to nanoemulsions is unclear. Indeed, nanoemulsions differ from emulsions formed from micrometer or larger droplets in the relative importance of entropic, electrostatic, and interfacial contributions to their elasticity[28–30]. To study the yielding of soft materials composed of nanoscale particles, optical techniques like DWS and microscopy are insufficient. However, coherent x-ray scattering, which accesses the nanoscale structural dynamics, has recently been employed in measurements of yielding soft materials composed of nanoscale particles subjected to LAOS[31,32]. This technique, which we call "LAOS-XPCS", is an extension of the coherent scattering method x-ray photon correlation spectroscopy (XPCS), which in general is a powerful approach for measuring the dynamical evolution of material microstructure relevant to rheology[33]. XPCS is the x-ray analog of dynamic light scattering (DLS), and it can characterize collective particle dynamics in a thermodynamically large ensemble over a range of nanometer-scale lengths determined by the wave-vector range of the measurement. In tandem with LAOS, XPCS measurements are therefore capable of extracting the length-scale dependence of shear-induced rearrangements during the yielding process.

The principle of LAOS-XPCS was demonstrated recently in a study of the irreversible microscopic restructuring of nanocolloidal gels under oscillatory shear[31]. The idea of the approach is the following: If a nominally static amorphous sample is subject to an oscillatory shear strain in an XPCS measurement, the motion of the particles due to the strain will change the speckle pattern and hence cause a decay in the intensity autocorrelation function $g_2(\mathbf{q}, t)$, where $\mathbf{q}$ is the scattering wave vector. However, after a complete cycle of an oscillatory strain, the scatterers will return to their original positions if the deformation is reversible, causing the speckle pattern to return to its original configuration. These echoes in the speckle pattern will thus cause $g_2(\mathbf{q}, t)$ to return to $g_2(\mathbf{q}, 0)$, and the correlation function will display peaks at integer multiples of the oscillation period (and minima at odd numbers of half cycles). On the other hand, if the shear induces irreversible rearrangements so that some particles do not return to their original positions, the peaks will be attenuated, and the reduction in amplitude will provide a measure of the microscopic irreversibility. This

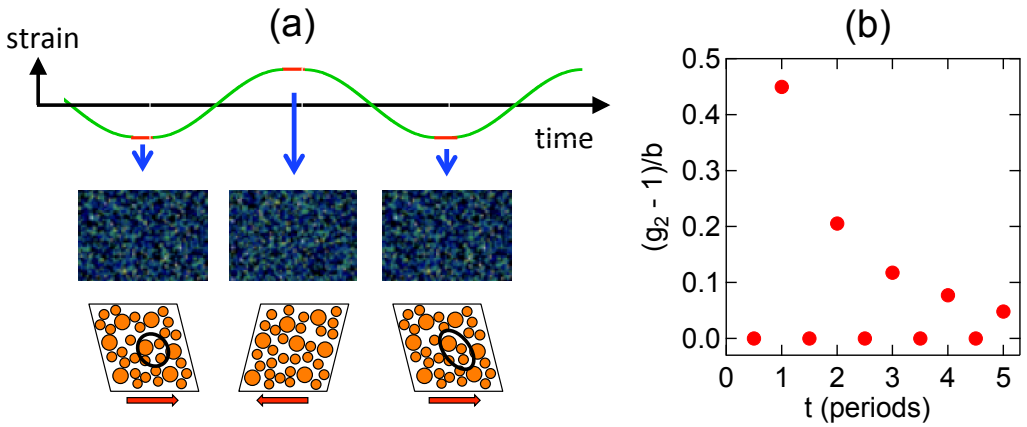

FIG. 1. (color online) (a) Schematic of the strain profile and microstructural response during XPCS measurements with LAOS. The strain follows a sinusoidal form between extrema (green). At each extremum the strain is held constant (red) for a short period during which a coherent x-ray exposure is obtained. Details from example speckle patterns are shown. The cartoons of the nanoemulsion illustrate the change in strain each half-period and the recovery of the microstructure each full period. The circled particles highlight a region that undergoes irreversible rearrangement during the cycle. (b) Schematic of correlation function resulting from such a measurement, where b is the Siegert factor.

measurement protocol is depicted schematically in Fig. 1(a). The strain follows a sinusoidal time dependence between extrema in its value. Upon arriving at each extremum, the strain is held constant while a scattering image is obtained. Periodically holding the strain fixed in this way eliminates "smearing" of the speckle pattern due to shearing of the sample during the x-ray exposures. The intensity autocorrelation function calculated for pairs of images separated by increasing numbers of cycles, depicted schematically in Fig. 1(b), reveals the wave-vector dependent attenuation in the echo peaks that characterizes the shear-induced structural dynamics associated with the irreversible displacements.

In the case of the nanocolloidal gels[31], this attenuation of the echo peaks had a sharp onset as a function of strain amplitude at a threshold strain $\gamma_c \approx 7\%$, indicating a transition to irreversible, nanoplastic deformation. The location of γ_c was near the yield point of the gels identified in macroscopic rheology. However, the gel rheology also displayed pronounced

deviations from linear elastic behavior at significantly lower strain amplitudes, indicating a range of strains where the response was nonlinear but the microscopic deformations were fully reversible. Further, analysis of the wave-vector dependence of the echo-peak attenuation above γ_c indicated that the irreversibility was associated with rearranging regions in the gels that had a power-law size distribution characteristic of a nonequilibrium critical transition at yielding.

In this paper we report a similar study on a set of concentrated nanoemulsions at different droplet volume fractions ϕ. This nanoemulsion series is an appealing system on which to apply LAOS-XPCS for several reasons. First, it offers a point of comparison with the nanocolloidal gels between soft disordered solids whose elasticity is a consequence of dominantly repulsive or dominantly attractive interactions. Second, as described below, by varying ϕ one can tune the nonlinear rheology and yielding behavior of the concentrated nanoemulsions, thus enabling a systematic comparison of macroscopic and microscopic signatures of yielding. Finally, the experiments allow us to compare the observed behavior with that seen in emulsions comprised of micrometer-scale droplets.

Section II below describes the set of nanoemulsions used in the study and the procedures employed in the LAOS-XPCS experiments, while Section III describes the results. In Section IV, we provide an interpretation for the shear-induced dynamics seen in the experiments, and Section V includes some concluding remarks. Briefly, we observe signatures of microscopic irreversibility in the XPCS measurements that increases at higher strain amplitudes in a way that correlates with the concentration-dependent rheological yielding of the nanoemulsions. The microscopic behavior near yielding shares features similar to those seen in the nanocolloidal gels including re-arrangement events with a power-law size distribution. Further, for lower-concentration nanoemulsions these events reveal evidence of memory under steady-state shear, wherein the locations of these events in a given cycle of strain are anti-correlated with those in recent previous cycles.

II. NANOEMULSION CHARACTERIZATION AND EXPERIMENTAL PROCEDURES

A. Synthesis and Structure

The nanoemulsions were composed of silicone oil droplets in water stabilized by sodium-dodecyl-sulfate (SDS). A nanoemulsion sample was prepared by forcing a pre-mixed oil-in-water emulsion composed of micrometer-scale droplets through a microfluidic Y-type channel at high pressures, leading to extensional and shear flows with peak strain rates as high as about 10^8 s^{-1}[34]. These extreme flow-driven excitations caused the larger droplets to rupture into nanoscale droplets. The nanoemulsion was then concentrated and its polydispersity was reduced through ultracentrifugal fractionation[1]. Through an evaporative gravimetric method, we measured $\phi = 0.653$ for this fractionated nanoemulsion. The average droplet radius and polydispersity were determined from measurements of the x-ray scattering form factor on a highly diluted suspension of the droplets, as shown in the inset to Fig. 2(a). The solid line through the data displays the result of a fit to the form factor based on a gaussian distribution of droplet sizes, which gave an average radius of 25.3 nm with a standard deviation of 12.2 nm.

Portions of this concentrated sample were diluted with appropriate amounts of aqueous SDS solution to create a series of four nanoemulsions with varying droplet volume fractions, $\phi = 0.439$, 0.500, 0.562, and 0.653, while keeping the bulk concentration of SDS fixed at 10 mM. Due to the ionic nature of SDS, the surfaces of the oil droplets were negatively charged, and the droplets interacted through a Coulombic repulsion with a Debye screening length of about $\lambda_D \approx 3.1$ nm, based on an approximation of a 10 mM monovalent salt concentration in the bulk. Because the Debye screening length was a non-negligible fraction of the average droplet radius, the nanoemulsion underwent a transition between fluid and elastic solid at a volume fraction below that expected for hard spheres, and at all four values of ϕ studied, the nanoemulsion was dominantly an elastic soft solid. In general, concentrated nanoemulsions pass through a series of regimes with increasing ϕ in which entropy, electrostatics, and interfacial forces in turn become the dominant contributor in imparting elasticity[30]. Based on the low-strain values of the nanoemulsions' elastic moduli, shown in Fig. 3 below, and the entropic-electrostatic-interfacial (EEI) model for the elasticity

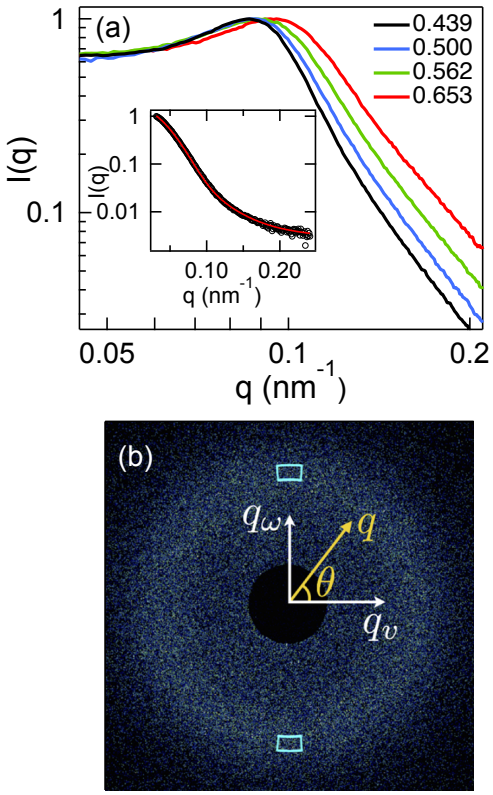

FIG. 2. (color online) (a) The normalized x-ray scattering intensity as a function of wave vector q for the four nanoemulsion concentrations in the study, as indicated in the legend. Inset: The normalized scattering intensity for a highly diluted nanoemulsion. The solid line in the inset displays a fit for the droplet form factor. (b) A CCD image of the coherent x-ray scattering intensity for the $\phi = 0.500$ nanoemulsion. The incident beam position, corresponding to $q = 0$, is obscured by the shadow of the beamstop in the center. The wave-vector directions parallel to the flow direction q_v and parallel to the vorticity direction q_ω are indicated by white arrows. Two examples of partitions along the vorticity direction that delineate the pixels included in the analysis of $g_2(q,t)$ at fixed wave-vector magnitude and direction are shown by areas enclosed in blue. These two partitions span 0.084 nm$^{-1} \leq q \leq$ 0.094 nm^{-1} and an azimuthal range of 10°.

of concentrated nanoemulsions[30], while also taking into account polydispersity, we infer that the nanoemulsions used in this study were in the interfacial regime, with the lowest concentration, $\phi = 0.439$, being near the border between the interfacial and electrostatic regimes.

B. LAOS-XPCS

LAOS-XPCS experiments were performed at beamline 8-ID-I of the Advanced Photon Source using 11 keV x-rays. During the measurements, the nanoemulsions were confined between two parallel plates of a custom shear cell. The spacing between the plates was 1.5 mm. Each plate was constructed using polycarbonate windows to allow for transmission small-angle scattering measurements. With the exception of a small area of the windows through which the x-rays passed, the windows in contact with the sample were abraded with sandpaper to prevent wall slip. The window downstream of the sample (relative to the x-ray beam) was held fixed, while the window upstream of the sample was attached to a translation stage driven by a voice-coil linear actuator. The software controlling the stage motion employed a PID feedback loop that monitored the stage position using an optical encoder with 50 nm precision and a 32 kHz refresh rate. The partially coherent x-ray beam incident on the samples was 20×20 μm^2 and was oriented normal to the windows and hence parallel to the shear-gradient direction. The small-angle-scattering wave vectors $\mathbf{q}$ therefore lay in the flow-vorticity plane. The scattering patterns were collected using a charge coupled device (CCD) area detector (ANL-BNL FastCCD) with a 960×962 pixel array located 4.91 m from the sample to span the range of wave-vector magnitudes 0.03 nm^{-1} $< q <$ 0.19 nm^{-1}. Figure 2(b) depicts a typical scattering image with wave vectors parallel to the flow direction, q_v, and parallel to the vorticity direction, q_ω, indicated. Figure 2(a) displays the normalized x-ray scattering intensity $I(q)$ of the four concentrated nanoemulsions obtained from averaging sequences of such images over wave-vector direction. The main change in $I(q)$ with droplet volume fraction is a shift to higher q of the structure factor peak near $q = 0.1$ nm^{-1}, indicating a decrease in nearest neighbor spacing with increasing ϕ. No measurable changes to $I(q)$ were observed due to the application of shear over the range of strain amplitudes covered in the LAOS-XPCS measurements.

Conventional XPCS measurements involve collecting sequences of images like that in Fig. 2(b) to obtain the coherent scattering intensity $I(\mathbf{q}, \tau)$ at times τ and calculating the intensity time autocorrelation function

$$g_2(\mathbf{q}, t) = \frac{\langle I(\mathbf{q}, \tau) I(\mathbf{q}, \tau + t) \rangle}{\langle I(\mathbf{q}, \tau) \rangle^2}, \tag{1}$$

where the averages are over τ and over detector pixels subtending a small range of wave vectors centered at $\mathbf{q}$. As depicted schematically in Fig. 1, in the LAOS-XPCS measurements

the nanoemulsions were subjected to oscillatory shear, and images of the coherent scattering intensity were collected stroboscopically in synchronization with the extrema of the strain. To prevent the smearing of speckles that would occur if images were captured during shear, the strain was briefly held constant at each extremum during the image acquisition. Specifically, the strain profile was composed of a sinusoidal shear at 0.318 Hz with a 0.6 s stoppage at each extremum, leading to an oscillation period $T = 4.34$ s. An x-ray image with 0.25 s exposure time was collected starting 0.3 s into each stoppage. Data sets therefore contained images separated by $T/2 = 2.17$ s. Typically, 128 images were obtained in each measurement to determine $g_2(\mathbf{q}, t)$. The XPCS measurements were performed in order of increasing strain amplitude. At each strain amplitude, the x-rays measurements were initiated several minutes after the start of the oscillatory shear (*i.e.*, after at least the first 100 cycles of shear). Thus, the correlations in coherent scattering intensity should be interpreted as a measure of the shear-induced structural dynamics occurring under steady-state LAOS.

As discussed above, the changes in the speckle pattern due to the shear were such that pairs of images taken at opposite extrema of the strain, $t = (n+1/2)T$ where n is an integer, were fully uncorrelated; *i.e.*, $g_2(\mathbf{q}, t) - 1 \approx 0$. Therefore, we focus on $g_2(\mathbf{q}, t)$ at delay times corresponding to integer values of the period, $t = nT$, which provides information about the degree of microscopic reversibility as a result of full cycles of LAOS. Furthermore, because the magnitude of $g_2(\mathbf{q}, t)$ decays especially rapidly with strain deformation at wave vectors parallel to the flow direction[32], we found that even the small residual differences in strain on each return of the shear cell to an extremum caused by the 50 nm resolution in plate position affected the amplitude of the echo peaks along q_v. Therefore, we focus our analysis on wave vectors centered around the vorticity direction and hence on the shear-induced dynamics perpendicular to the direction of affine strain. Specifically, the detector pixels were partitioned into regions of varying wave-vector magnitude over an angular spread of $\pm 5^\circ$ about q_ω for averaging to obtain $g_2(q, t)$. For example, the blue boxes in Fig. 2(b) show the partition corresponding to $q \approx 0.09$ nm^{-1}.

C. Rheology

Measurements of the shear rheology of the four nanoemulsions were performed using a stress-controlled rheometer (Anton-Paar MCR 300) in a cone-and-plate geometry. A varnish

containing fine-grit sand was applied to the tool surfaces to prevent slip. The temperature, controlled using a Peltier stage, was held at 27 °C for all measurements. Figure 3(a) shows the complex shear modulus $G^*(\nu) = G'(\nu) + iG''(\nu)$ at frequency $\nu = 0.318$ Hz as a function of strain amplitude γ for each nanoemulsion. The moduli possess characteristics typical of disordered soft solids. In the linear viscoelastic region at low strain amplitude, the nanoemulsions respond as elastic solids, with G' and G'' roughly constant and $G' \gg G''$. At higher amplitude, the response becomes nonlinear and reveals characteristics of yielding. The storage modulus decreases monotonically, while the loss modulus goes through a maximum associated with a "weak strain overshoot"[35]. At a strain amplitude above the G'' maximum, G' and G'' intersect. This intersection point, which we define as γ_f, is where the viscous response of the material starts to dominate the elastic response and is nominally where bulk fluidization occurs.

The strain-dependent trends in the effective shear moduli displayed in Fig. 3(a) are common to many soft glassy systems[35] including concentrated colloidal gels, as illustrated in the previous LAOS-XPCS study mentioned above. (Compare Fig. 3 with Fig. 1 in Ref.[31].) These similarities exist despite the different microscopic mechanisms instilling elasticity to the materials, *e.g.*, the colloidal gels possess rigid, system-spanning backbones of particles aggregated through attractive interactions, while the emulsion elasticity derives from the jammed configuration of the repulsively interacting droplets, and the materials' differing microstructures, wherein the gels are characterized by a hierarchical structure of particle-rich regions and voids, while deformable emulsion droplets can achieve effective densities exceeding random close packing. A key question we address in the present LAOS-XPCS study is the extent to which these macroscopic similarities in the yielding and flow behavior are mirrored by their microscopic signatures.

While γ_f, defined as the crossing point of G' and G'', provides a measure of the strain amplitudes required to induce fluid-like response from the nanoemulsions, yielding is typically associated with the onset of nonlinear behavior that occurs at lower strain, and several alternative criteria for identifying the yield strain have been proposed. Figure 3(b) shows the strain dependence of the product $G'\gamma$, known as the elastic stress, which is a representation of the strain-dependent rheology that facilitates identification of points of yielding[36]. Above a linear regime at low strain, where $G'\gamma$ is proportional to γ, the stress-strain relation becomes sublinear, and $G'\gamma$ reaches a maximum. Such maxima are common in the

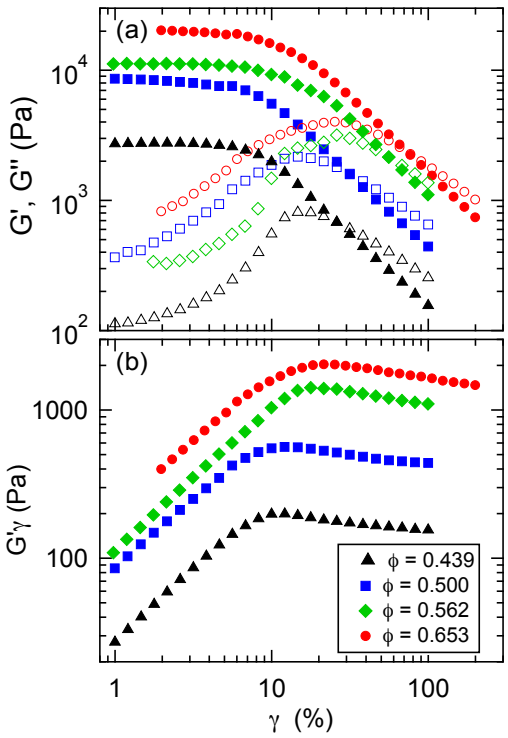

FIG. 3. (color online) (a) Storage (solid symbols) and loss (open symbols) moduli measured at $\nu = 0.318$ Hz as a function of strain amplitude for four droplet volume fractions of the same concentrated emulsion at $\phi = 0.439$ (triangles), 0.500 (squares), 0.562 (diamonds), and 0.653 (circles). (b) Elastic stress at $\nu = 0.318$ Hz as a function of strain amplitude for the four droplet volume fractions.

rheology of disordered soft solids, and their position, which we define as γ_y, is often used to locate the yield point. Both γ_f and γ_y increase systematically with increasing ϕ, as shown in Fig. 4, which displays the values for the four nanoemulsions. This dependence follows the one expected upon increasing concentration above jamming, the point where the system forms a marginally connected solid, to higher volume fractions where droplet motion is increasingly over-constrained. Indeed, a recent model for emulsion elasticity by Scheffold *et al.*[28] that takes into account changes in the droplet interactions and the connectivity of the stress-bearing network above jamming predicts $\gamma_y = a(\phi/\phi_j - 1)^{0.7}$, where ϕ_j is the jamming volume fraction and $a \approx 0.2$ [37]. The solid line in Fig. 4 shows the result of a fit to γ_y using this form, which gives $\phi_j = 0.35 \pm 0.02$ and $a = 0.23 \pm 0.03$ in good agreement with the

model. A major objective of the LAOS-XPCS measurements described below is to track how the microscopic irreversibility in droplet displacements correlates with these observed trends in macroscopic yielding and flow behavior as ϕ is varied.

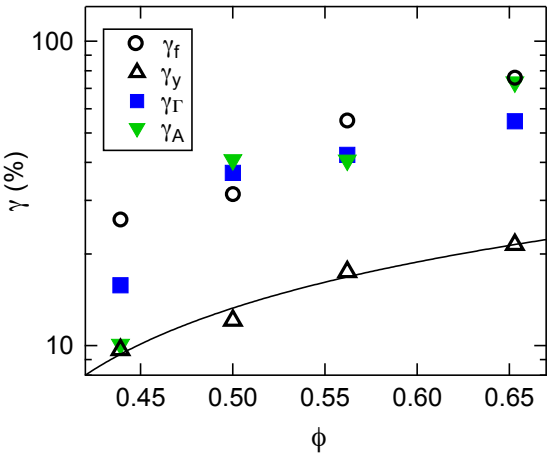

FIG. 4. (color online) Strain amplitudes at which features of yielding appear as a function of droplet volume fraction. Included from the macroscopic rheometry are γ_f, the strain at which G' and G'' intersect, and γ_y, the strain at which the elastic stress reaches a maximum. Also plotted are the strains at which two features in the LAOS-XPCS measurements indicate a sharp rise in microscopic irreversibility, the strain γ_Γ at which Γ crosses 0.2 cycles^{-1} and the strain γ_A at which the overall echo peak amplitude A drops below 0.1.

III. RESULTS

Figures 5(a) and (b) display $g_2(q, n)$ at $q = 0.09$ nm^{-1}, which is near the structure factor peak in $I(q)$, for the nanoemulsions with $\phi = 0.500$ and 0.653, respectively, at various strain amplitudes. Here, the integer n denotes the number of "lag cycles"; that is, the number of cycles separating the pairs of images employed in calculating $g_2(q, n)$ and therefore the effective delay time over which shear-induced dynamics occurs under the steady-state LAOS. The general features of the correlation functions of the other nanoemulsions were similar to those in Fig. 5. At sufficiently small strains, $g_2(q, n)$ maintained a large, roughly constant value as a function of n, as illustrated by the results at $\gamma = 2\%$ in Fig. 5(a), indicating that any relative displacement of the droplets during the oscillatory strain at these amplitudes

was reversible. However, at larger strains, such as at $\gamma = 28\%$ in Fig. 5(a), $g_2(q, n)$ decayed appreciably with n, indicating irreversibility in the droplet displacements. To model this decay we fit the correlations to a compressed exponential function,

$$g_2(q, n) - 1 = Ae^{-(\Gamma n)^\beta} \tag{2}$$

where A is the amplitude, Γ is the decay rate, and β is the shape parameter. The lines in Fig. 5 show the results of these fits. In many cases, $g_2(q, n)$ was described by a simple exponential, $\beta = 1$, and the dashed lines in Fig. 5 display fit results in which β was held fixed equal to one. In particular, at the highest concentration, $\phi = 0.653$, the decay in $g_2(q, n)$ was described by a simple exponential at all strains and wave vectors. (See, e.g., Fig. 5(b).) However, at lower concentrations, deviations from a simple exponential decay were apparent. These deviations were most obvious at $\phi = 0.500$, where $g_2(q, n)$ at $\gamma < 32\%$ was significantly compressed. The solid lines in Fig. 5(a) display results of fits using a compressed exponential line shape, in which the average value of the shape parameter was $\beta = 1.53 \pm 0.20$. To within the certainty with which β could be determined, this average value was independent of wave vector. A similar trend was also observed at low strain amplitude ($\gamma < 16\%$) in the lowest-concentration nanoemulsion, $\phi = 0.439$, although the rapid decay and small amplitude of $g_2(q, n)$ at this concentration led to larger uncertainty in β. An interpretation for these simple-exponential and compressed-exponential lineshapes is given in the Discussion section below.

Figure 6(a) displays the decay rate Γ obtained from fits to $g_2(q, n)$ as a function of strain amplitude for each of the four concentrations. At all ϕ the decay rate maintains a small, approximately constant value at small strains before rising rapidly at larger strain. We associate the slow decay at low strains with intrinsic dynamics in the nanoemulsions probed by XPCS under quiescent conditions[38] and not with any shear-induced dynamics. The rise in Γ at larger strains, however, indicates a pronounced microscopic irreversibility in the strain response of the nanoemulsions and hence an onset of plastic deformation. A discussion of the microscopic nature of these dynamics is given in Section IV below. Here, we note simply that the increase in Γ occurs over a range of strain amplitudes that depends strongly on nanoemulsion concentration, with the increase occurring at larger γ for larger ϕ. To identify the strain value at which Γ begins to rise and hence the onset of irreversibility, we define a threshold strain γ_Γ as the strain at which $\Gamma = 0.2$ cycles^{-1}. While this definition

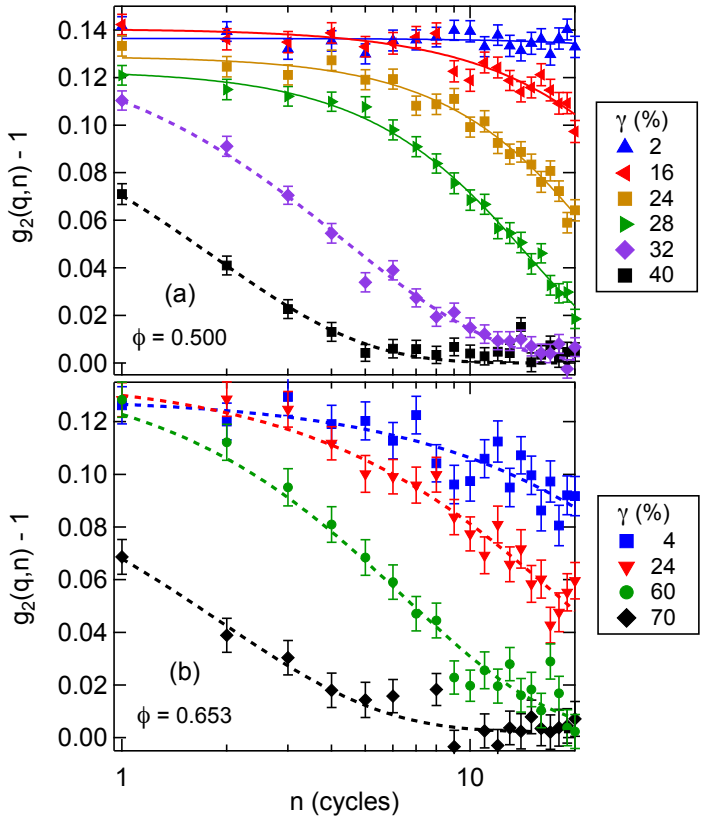

FIG. 5. (color online) Echo peaks at $q = 0.09$ nm^{-1} as a function of lag cycle n for nanoemulsions with (a) $\phi = 0.500$ and (b) $\phi = 0.653$. The dashed lines depict the results of fits to the data using Eq. 2 with $\beta = 1$, while the solid lines in (a) are from fits with β as a free parameter. Specifically, for $\phi = 0.500$, the fits give $\beta = 1.3$, 1.7, and 1.6 at $\gamma = 16\%$, 24%, and 28%, respectively.

is admittedly arbitrary, the sharp increase of Γ with γ that each nanoemulsion displays indicates that the precise definition is not crucial. The value of γ_Γ for each ϕ is plotted in Fig. 4.

Roughly coincident with the increase in Γ with γ, the amplitude A of the decay in $g_2(q, n)$ undergoes a sharp decrease, as seen in Fig. 6(b). In principle, the amplitude of the decay in $g_2(q, t)$ is given by the Siegert factor b, which we determined from separate measurements on a static sample (aerogel) to be $b \approx 0.14$. (We note that realignment of the x-ray optics between measurements on the different samples led to slight variations in b between each sample, but the value remained close to 0.14.) The suppression of A below the Siegert factor with increasing γ, which is seen with all the nanoemulsions, indicates a partial decay

of $g_2(q,t)$ that results from short-range droplet motion occurring within each oscillation period. A discussion of the microscopic nature of these dynamics is again given in Section IV below. To identify the strain amplitude where these dynamics affect $g_2(q,n)$ appreciably, we define another threshold strain γ_A as the strain at which $A = 0.10$. Again, while this definition is arbitrary, the sharp decrease of A with γ indicates that the precise definition is not crucial.

The values of γ_A are included in Fig. 4 along with γ_Γ and the yield strains γ_y and flow strains γ_f identified from rheology. As a function of ϕ, the strain values identified in the XPCS measurements as marking the onset of microscopic shear-induced dynamics track the strain values marking features of the nonlinear rheology. At the three largest ϕ, the onset of microscopic irreversible dynamics is closer to γ_f than to γ_y, implying a large range of strains in which the rheological response was nonlinear but the deformations were essentially reversible[20,39–41]. In contrast, the microscopic onset of irreversibility in the lowest-concentration nanoemulsion, $\phi = 0.439$, occurs closer to γ_y. As mentioned above, the lowest-concentration sample was at the border between the interfacial and electrostatic regimes of nanoemulsion elasticity[30], while the higher-concentration samples were deep in the interfacial regime where the droplets are strongly jammed, indicating that the onset of microscopic irreversibility could be sensitive to the interparticle interactions. This picture is complicated, however by the microscopy experiments on concentrated emulsions composed of micrometer-scale droplets, in which Knowlton *et al.* observed an onset of irreversible droplet displacements at a strain that was coincident with the onset of nonlinear rheology and thus more similar to the behavior of the lowest-concentration nanoemulsion[27]. This difference could be a consequence of the differing microscopic properties of nanoemulsions versus emulsions of micrometer-scale droplets but could also result from the differing types of dynamics probed in the microscopy versus XPCS measurements. Specifically, the particle-tracking methods in the microscopy measured absolute self-displacements of the droplets, while the XPCS measurements probe collective motion, potentially making the two techniques sensitive to different aspects of irreversibility under LAOS.

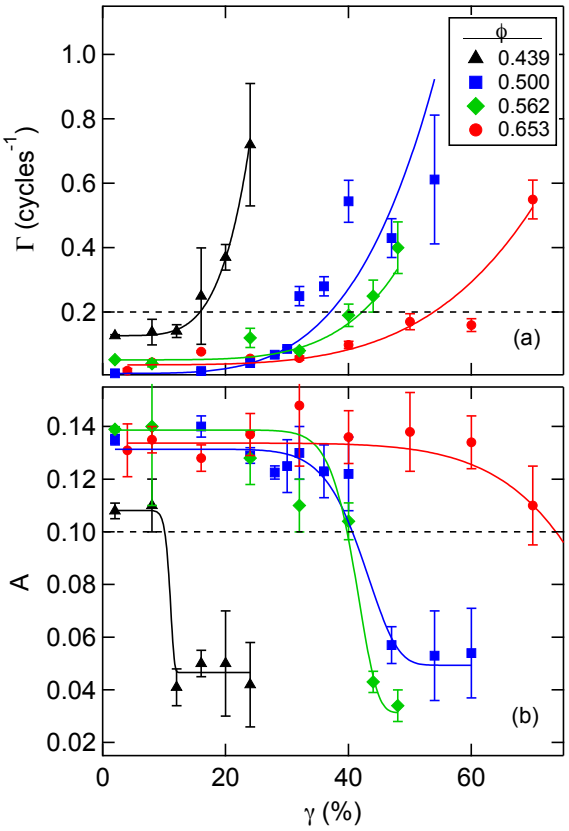

FIG. 6. (color online) The (a) decay rate Γ and (b) amplitude A extracted from fits to the echo peaks using Eq. (2) at different droplet concentrations as indicated in the legend at $q = 0.09$ nm^{-1} as a function of strain amplitude. The solid lines are guides to the eye. The dashed lines in (a) and (b) denote $\Gamma = 0.2$ and $A = 0.10$, respectively, the values used to identify the characteristic strains γ_Γ and γ_A.

IV. DISCUSSION

As described above, two features in the attenuation of the echoes in the LAOS-XPCS measurements correlate with the macroscopic yielding and fluidization of the nanoemulsions. The first is the exponential or compressed exponential decay in the correlation function with decay rate Γ that increases rapidly at high strain, and the second is the overall amplitude A of the correlation function, which decreases at high strain. Here, we discuss interpretations for the shear-induced microscopic structural dynamics responsible for these features. While a quasi-exponential decay of the correlation function is suggestive of effective diffusion

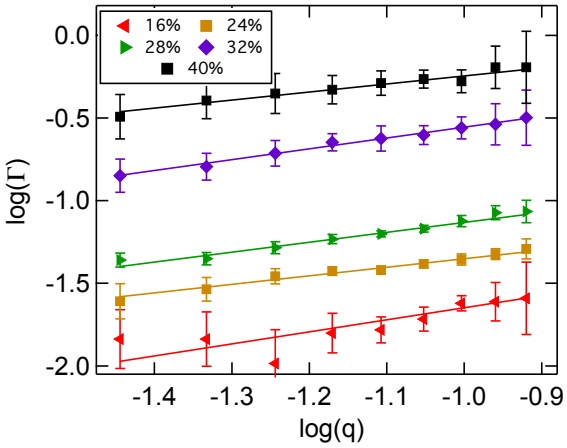

FIG. 7. (color online) Echo-peak decay rate as a function of wave-vector amplitude for the nanoemulsion with $\phi = 0.500$ at various strain amplitudes, as indicated in the legend. The solid lines are the results of power-law fits that give power-law exponents in the range $\alpha = 0.49$ to 0.73.

dynamics of the nanoemulsion droplets in response to the shear, and indeed shear-induced diffusion has been identified in simulations and microscopy experiments of sheared colloidal glasses[42–46], we can discount such an interpretation based on the wave-vector dependence of Γ. For diffusion, the decay rate would vary with wave vector as $\Gamma \sim q^2$, perhaps modulated by the structure factor $S(q)$ in analogy with de Gennes narrowing. Figure 7 displays Γ as a function of q for the nanoemulsion with $\phi = 0.500$ at various strain amplitudes. In contrast with expectations for diffusion, Γ follows a much weaker dependence on q. At all amplitudes, the decay rates scale as a weak power law, $\Gamma(q) \sim q^{\alpha}$. The value of α varies slightly with no systematic trend, perhaps as a consequence of sample heterogeneity, but is consistently less than one. The average value for the nanoemulsion with $\phi = 0.500$ is $\alpha = 0.60 \pm 0.10$. Weak power-law behavior with similar values of α was observed with the other nanoemulsions. The value of α averaged over all ϕ and all γ at which the exponent could be confidently obtained was $\alpha = 0.70 \pm 0.15$.

Notably, this value of the exponent, $\alpha = 0.70$, is essentially the same as was found in the previous LAOS-XPCS study of nanocolloidal gels, where the correlation functions displayed simple exponential decays at all strain amplitudes above yielding[31]. To explain these results in the gels, we developed a model of heterogeneous shear-induced dynamics, described in detail in Ref.[31], in which some regions of the gel underwent irreversible rearrangements each

cycle while the rest of the gel deformed reversibly. Within this model, the exponential decay of $g_2(q,n)$ implied the rearranging regions were located randomly, unbiased by the locations in previous cycles, and the scaling of Γ with q implied that the volumes V of the rearranging regions had a power-law distribution, $N(V) \sim V^{-\xi}$ with $\xi = (\alpha + 4)/3 = 1.56$, indicating a nonequilibrium critical transition at yielding.[31]. (On the other hand, according to the model if the regions that re-arrange in a given cycle are more likely than average to re-arrange in a subsequent cycle, $g_2(q,n)$ would be stretched, while if those regions were less likely than average, $g_2(q,n)$ would be compressed.)

The same weak power-law behavior seen in Fig. 7 indicates that the yielding of the nanoemulsions is characterized microscopically by a similar power-law distribution of rearranging regions. This commonality in the microscopic signatures of yielding in the gels and nanoemulsions might seem surprising given that the elasticity of the gels derives from a network of attractive colloidal bonds while the repulsive nanoemulsions are in a jammed state; however, as note above, the two systems display qualitatively similar plastic-like yielding behavior in their rheology. (Compare Fig. 3 with Fig. 1 in Ref.[31].) Further, similar power-law distributions have been observed in the nonlinear mechanical response in a range of disordered systems[47–58]. These power-law distributions of event sizes that are shared by the nanocolloidal gels and concentrated nanoemulsions further suggest that yielding in the systems should be considered a nonequilibrium critical transition. We note, however, that the sharp onset of the irreversibility seen in both systems, as illustrated particularly by the drop in A seen in Fig. 6(b), also suggests a discontinuous onset of plasticity that would be consistent with a first-order-like transition as suggested in recent studies of colloidal glasses under LAOS[18,19,46].

A subtle difference between the results in the nanoemulsions and those in the gels, however, is the deviations from simple exponential decays of $g_2(q,n)$ that are apparent at smaller ϕ. In particular, within the model of heterogeneous shear-induced dynamics described above, non-exponential lineshapes in $g_2(q,n)$ imply spatial correlations among the irreversible rearrangements during different cycles. Specifically, a faster-than-exponential decay of the correlations ($\beta > 1$) indicates a bias toward rearrangements during a given cycle of shear occurring in regions that have *not* undergone rearrangement in a recent previous cycle. The reason that such bias is apparently more pronounced in the lower-concentration nanoemulsions is not immediately clear. As mentioned above, one notable difference between the lower- and

higher-concentration nanoemulsions is the relative importance of entropy, electrostatics, and interfacial forces in dictating the elasticity, which could lead to differing nonlinear mechanical response. Further, we speculate that the bias seen in the lower-concentration nanoemulsions could be related to the broadening in the distribution of inter-droplet forces in emulsions that is observed as the concentration is reduced toward the jamming point[59,60]. Specifically, if one assumes that the heterogeneity in inter-droplet forces dictates which regions are most susceptible to yielding, and that the yielding events alter the spatial structure of this heterogeneity, one might expect that regions that re-arrange would have reduced probability of re-arranging again.

Regarding the effect of shear on the overall amplitude A of the correlation functions, as mentioned above, the decrease in A at high strain amplitudes is a sign of short-range droplet motion that acts in parallel with the heterogeneous rearrangement events to cause a partial decay in $g_2(q, n)$. Specifically, when the droplets in a re-arranging region alter their relative positions in a given cycle, they necessitate droplet motion in the surrounding nanoemulsion; that is, in regions that do not undergo rearrangement during the cycle. One interpretation for this motion is that it resembles the localized "caged" dynamics seen in glasses, wherein particles move within the restricted volumes defined by the interactions with their neighbors in the disordered packing. When this motion occurs on time scales that are too fast to access in a correlation spectroscopy measurement, it leads to a Debye-Waller-like suppression in the short-time plateau value of $g_2(q, t)$ such that $A \sim \exp(-r_0^2 q^2/6)$, where r_0^2 is the mean squared displacement of the localized or caged motion[61,62]. Figure 8 shows A plotted on a log scale against q from measurements at two strain amplitudes on the nanoemulsions with $\phi = 0.439$ and $\phi = 0.500$ along with a fit to the results using this form. The observed wave-vector dependence of A is indeed consistent with such localized displacements. We note that in the absence of shear no such wave-vector-dependent suppression in the amplitude of $g_2(q, t)$ is observed, indicating that any thermally-driven localized droplet motion is severely restricted. Within this interpretation, then, the shear strain and the re-arrangement events that it triggers act like a large effective temperature to drive the caged dynamics.

While this picture of caged dynamics is consistent with the data, it is based on the idea that the droplets move randomly with respect to their neighbors. An alternative interpretation that we believe is more plausible for the highly elastic nanoemulsions identifies the short-range dynamics instead with strain displacements. Specifically, when a re-arrangement

event occurs, it necessitates a redistribution of the stress in the surrounding nanoemulsion. The strain in response to this change in the stress field can be expressed as an expansion in moments that on large length scales will be dominated by the lowest-order non-zero moment. Because the droplets are incompressible, the re-arrangement events should be essentially volume conserving, and hence the monopole term should vanish so that the leading term is dipolar. Such dipolar strain fields create a distribution of local displacements u that decays as $u^{-5/2}$, which has a diverging variance and which calculations have shown leads to anomalous wave-vector dependence in the resulting correlation function[63–65]. Specifically, strain displacements that are sufficiently small to cause a partial decay in $g_2(q,t)$ lead to a wave-vector dependent plateau value $A \sim \exp(-(\lambda q)^{3/2})$, where λ depends on factors such as the density and strength of the stress dipoles and the elasticity of the medium. As a test of whether such motion is also consistent with the partial decays in $g_2(q,n)$ of the nanoemulsions under shear, Fig. 8 displays the result of a second fit to the data using this form. As the figure indicates, the observed wave-vector dependence of A is consistent with such strain displacements; however, the scatter in the data is too large for the results to distinguish between strain and caged dynamics as the microscopic mechanism causing the suppression of A. Finally, we note that inspection of the echo-peak amplitudes in the LAOS-XPCS measurements on the nanocolloidal gels[31] indicates partial decays were also present in those results but were smaller than those affecting the correlations in the nanoemulsions. This difference between the gels and nanoemulsions is presumably a consequence of the difference in how stress redistributes in response to restructuring in the gel networks (where stress is exclusively transmitted through strands of bonded particles) versus in the jammed nanoemulsions (where stress can be communicated between all locally jammed particles).

V. CONCLUSION

In conclusion, LAOS-XPCS measurements on a series of concentrated nanoemulsions have revealed signatures of microscopic dynamics associated with plastic events that result in irreversible droplet re-arrangements. The threshold strains for these events correlate with features in the macroscopic rheology that signal nonlinear mechanical response of the nanoemulsions. These threshold strains lie below the strains γ_f at which the nanoemulsions become effectively fluidized, but, except for the lowest-concentration nanoemulsion, they

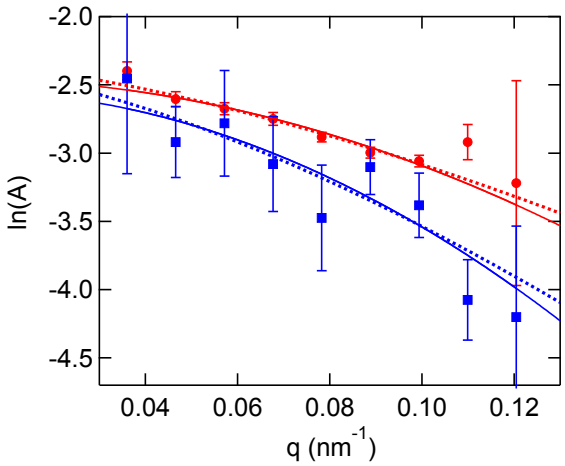

FIG. 8. (color online) The overall correlation amplitude A plotted on a log scale as a function of wave vector for the nanoemulsion with $\phi = 0.500$ at $\gamma = 55\%$ (blue squares) and for the nanoemulsion with $\phi = 0.493$ at $\gamma = 12\%$ (red circles). The solid lines are the results of fits to the data using the form $A \sim \exp(-r_0^2 q^2/6)$, and the dashed lines are fits using $A \sim \exp(-(\lambda q)^{3/2})$.

also lie significantly above the onset strain for nonlinear rheological response. This observed robustness to irreversible re-arrangements could be a consequence of the experimental protocol in which the nanoemulsions have been subjected to many cycles of LAOS prior to the XPCS measurements. Indeed, simulations and experiments on amorphous solids [39,46,66–68] have detected transient behavior at the start-up of LAOS during which the amount of irreversible microscopic particle displacement decreases. Our interpretation for the compressed exponential lineshapes of $g_2(q,n)$ in terms of a bias against regions that re-arrange during a given cycle re-arranging again during a subsequent cycle indicates that the nanoemulsion microstructure can possess a degree of memory of the mechanical history that would be consistent with the ability to train the nanoemulsions against plastic failure. This notion of history-dependent structure and material memory is qualitatively consistent with experiments by Huang and Mason involving time-resolved angle-dependent light scattering from concentrated microscale emulsions subjected to LAOS[24,25]. Further XPCS experiments on nanoemulsions and other nanostructured soft solids that focus on transient effects in the microscopic irreversibility during the start-up of LAOS and that can correlate these effects with possible history-dependent rheology would provide insight into this aspect of their

mechanical behavior.

VI. ACKNOWLEDGEMENTS

Funding was provided by NSF Grant Nos. CBET-1336166 and CBET-1804721 and the NSERC Discovery grant program. TGM and MJP acknowledge financial support from UCLA. This research used resources of the Advanced Photon Source, a U.S. Department of Energy (DOE) Office of Science User Facility operated for the DOE Office of Science by Argonne National Laboratory under Contract No. DE-AC02-06CH11357.

---

* jharden@uottawa.ca

† leheny@jhu.edu

[1] T. G. Mason, J. N. Wilking, K. Meleson, C. B. Chang, and S. M. Graves, "Nanoemulsions: formation, structure, and physical properties," J. Phys.: Condens. Matter **18**, R635 (2006).

[2] M. L. Falk and J. S. Langer, "Deformation and failure of amorphous, solidlike materials," Annu. Rev. Condens. Matter Phys. **2**, 353 (2011).

[3] A. P. R. Eberle and L. Porcar, "Flow-SANS and rheo-SANS applied to soft matter," Curr. Opin. Colloid Interface Sci. **17**, 33 – 43 (2012).

[4] R. G. Egres, F. Nettesheim, and N. J. Wagner, "Rheo-SANS investigation of acicular-precipitated calcium carbonate colloidal suspensions through the shear thickening transition," J. Rheol. **50**, 685–709 (2006).

[5] S. Rogers, J. Kohlbrecher, and M. P. Lettinga, "The molecular origin of stress generation in worm-like micelles, using a rheo-SANS LAOS approach," Soft Matter **8**, 7831–7839 (2012).

[6] I. Bihannic, C. Baravian, J. F. L. Duval, E. Paineau, F. Meneau, P. Levitz, J. P. de Silva, P. Davidson, and L. J. Michot, "Orientational order of colloidal disk-shaped particles under shear-flow conditions: a rheological–small-angle x-ray scattering study," J. Phys. Chem. B **114**, 16347–16355 (2010).

[7] M. P. Lettinga, P. Holmqvist, P. Ballesta, S. Rogers, D. Kleshchanok, and B. Struth, "Nonlinear behavior of nematic platelet dispersions in shear flow," Phys. Rev. Lett. **109**, 246001 (2012).

[8] C. R. López-Barrón, L. Porcar, A. P. R. Eberle, and N. J. Wagner, "Dynamics of melting and recrystallization in a polymeric micellar crystal subjected to large amplitude oscillatory shear flow," Phys. Rev. Lett. **108**, 258301 (2012).

[9] A. M. Philippe, C. Baravian, M. Jenny, F. Meneau, and L. J. Michot, "Taylor-couette instability in anisotropic clay suspensions measured using small-angle x-ray scattering," Phys. Rev. Lett. **108**, 254501 (2012).

[10] F. E. Caputo, W. R. Burghardt, K. Krishnan, F. S. Bates, and T. P. Lodge, "Time-resolved small-angle x-ray scattering measurements of a polymer bicontinuous microemulsion structure factor under shear," Phys. Rev. E **66**, 041401 (2002).

[11] L. M. C. Dykes, J. M. Torkelson, and W. R. Burghardt, "Shear-induced orientation in well-exfoliated polystyrene/clay nanocomposites," Macromolecules **45**, 1622–1630 (2012).

[12] A. P. R. Eberle, N. Martys, L. Porcar, S. R. Kline, W. L. George, J. M. Kim, P. D. Butler, and N. J. Wagner, "Shear viscosity and structural scalings in model adhesive hard-sphere gels," Phys. Rev. E **89**, 050302 (2014).

[13] J. Min Kim, A. P. R. Eberle, A. K. Gurnon, L. Porcar, and N. J. Wagner, "The microstructure and rheology of a model, thixotropic nanoparticle gel under steady shear and large amplitude oscillatory shear (laos)," J. Rheol. **58**, 1301–1328 (2014).

[14] J. Kim, D. Merger, M. Wilhelm, and M. E. Helgeson, "Microstructure and nonlinear signatures of yielding in a heterogeneous colloidal gel under large amplitude oscillatory shear," J. Rheol. **58**, 1359–1390 (2014).

[15] P. Varadan and M. J. Solomon, "Shear-induced microstructural evolution of a thermoreversible colloidal gel," Langmuir **17**, 2918–2929 (2001).

[16] H. Hoekstra, J. Mewis, T. Narayanan, and J. Vermant, "Multi length scale analysis of the microstructure in sticky sphere dispersions during shear flow," Langmuir **21**, 11017–11025 (2005).

[17] O. Korculanin, D. Hermida-Merino, H. Hirsemann, B. Struth, S. A. Rogers, and M. P. Lettinga, "Anomalous structural response of nematic colloidal platelets subjected to large amplitude stress oscillations," Phys. Fluids **29**, 023102 (2017).

[18] M. T. Dang, D. Denisov, B. Struth, A. Zaccone, and P. Schall, "Reversibility and hysteresis of the sharp yielding transition of a colloidal glass under oscillatory shear," Eur. Phys. J. E **39**, 44 (2016).

[19] D. V. Denisov, M. T. Dang, B. Struth, A. Zaccone, G. H. Wegdam, and P. Schall, "Sharp symmetry-change marks the mechanical failure transition of glasses," Sci. Rep. **5**, 14359 (2015).

[20] N. C. Keim and P. E. Arratia, "Mechanical and microscopic properties of the reversible plastic regime in a 2D jammed material," Phys. Rev. Lett. **112**, 028302 (2014).

[21] P. Hébraud, F. Lequeux, J. P. Munch, and D. J. Pine, "Yielding and rearrangements in disordered emulsions," Phys. Rev. Lett. **78**, 4657–4660 (1997).

[22] M. Laurati, S. U. Egelhaaf, and G. Petekidis, "Plastic rearrangements in colloidal gels investigated by laos and ls-echo," J. Rheol. **58**, 1395–1417 (2014).

[23] S. Aime, L. Ramos, and L. Cipelletti, "Microscopic dynamics and failure precursors of a gel under mechanical load," Proc. Natl. Acad. Sci. U. S. A. **115**, 3587–3592 (2018).

[24] J.-R. Huang and T. G. Mason, "Shear oscillation light scattering of droplet deformation and reconfiguration in concentrated emulsions," EPL **83**, 28004 (2008).

[25] J.-R. Huang and T. G. Mason, "Deformation, restructuring, and un-jamming of concentrated droplets in large-amplitude oscillatory shear flows," Soft Matter **5**, 2208 (2009).

[26] J. Clara-Rahola, T. A. Brzinski, D. Semwogerere, K. Feitosa, J. C. Crocker, J. Sato, V. Breedveld, and E. R. Weeks, "Affine and nonaffine motions in sheared polydisperse emulsions," Phys. Rev. E **91**, 010301 (2015).

[27] E. D. Knowlton, D. J. Pine, and L. Cipelletti, "A microscopic view of the yielding transition in concentrated emulsions," Soft Matter **10**, 6931–6940 (2014).

[28] F. Scheffold, J. N. Wilking, J. Haberko, F. Cardinaux, and T. G. Mason, "The jamming elasticity of emulsions stabilized by ionic surfactants," Soft Matter **10**, 5040–5044 (2014).

[29] T. G. Mason and F. Scheffold, "Crossover between entropic and interfacial elasticity and osmotic pressure in uniform disordered emulsions," Soft Matter **10**, 7109–7116 (2014).

[30] H. S. Kim, F. Scheffold, and T. G. Mason, "Entropic, electrostatic, and interfacial regimes in concentrated disordered ionic emulsions," Rheol. Acta **55**, 683–697 (2016).

[31] M. C. Rogers, K. Chen, L. Andrzejewski, S. Narayanan, S. Ramakrishnan, R. L. Leheny, and J. L. Harden, "Echoes in x-ray speckles track nanometer-scale plastic events in colloidal gels under shear," Phys. Rev. E **90**, 062310 (2014).

[32] R. L. Leheny, M. C. Rogers, K. Chen, S. Narayanan, and J. L. Harden, "Rheo-XPCS," Curr. Opin. Colloid Interface Sci. **20**, 261 – 271 (2015).

[33] R. L. Leheny, "XPCS: Nanoscale motion and rheology," Curr. Opin. Colloid Interface Sci. **17**, 3–12 (2012).

[34] K. Meleson, S. Graves, and T. G. Mason, "Formation of concentrated nanoemulsions by extreme shear," Soft Matter **2**, 109 (2004).

[35] K. Hyun, M. Wilhelm, C. O. Klein, K. S. Cho, J. G. Nam, K. H. Ahn, S. J. Lee, R. H. Ewoldt, and G. H. McKinley, "A review of nonlinear oscillatory shear tests: Analysis and application of large amplitude oscillatory shear (LAOS)," Prog. Polym. Sci. **36**, 1697 (2011).

[36] M. Laurati, S. U. Egelhaaf, and G. Petekidis, "Nonlinear rheology of colloidal gels with intermediate volume fraction," J. Rheol. **55**, 673–706 (2011).

[37] F. Scheffold, F. Cardinaux, and T. G. Mason, "Linear and nonlinear rheology of dense emulsions across the glass and the jamming regimes," J. Phys.: Condens. Matter **25**, 502101 (2013).

[38] H. Guo, J. N. Wilking, D. Liang, T. G. Mason, J. L. Harden, and R. L. Leheny, "Slow, nondiffusive dynamics in concentrated nanoemulsions," Phys. Rev. E **75**, 041401 (2007).

[39] I. Regev, T. Lookman, and C. Reichhardt, "Onset of irreversibility and chaos in amorphous solids under periodic shear," Phys. Rev. E **88**, 062401 (2013).

[40] D. Fiocco, G. Foffi, and S. Sastry, "Oscillatory athermal quasistatic deformation of a model glass," Phys. Rev. E **88**, 020301 (2013).

[41] N. V. Priezjev, "Reversible plastic events during oscillatory deformation of amorphous solids," Phys. Rev. E **93**, 013001 (2016).

[42] K. Miyazaki, D. R. Reichman, and R. Yamamoto, "Supercooled liquids under shear: Theory and simulation," Phys. Rev. E **70**, 011501 (2004).

[43] R. Besseling, E. R. Weeks, A. B. Schofield, and W. C. K. Poon, "Three-dimensional imaging of colloidal glasses under steady shear," Phys. Rev. Lett. **99**, 028301 (2007).

[44] D. Chen, D. Semwogerere, J. Sato, V. Breedveld, and E. R. Weeks, "Microscopic structural relaxation in a sheared supercooled colloidal liquid," Phys. Rev. E **81**, 011403 (2010).

[45] N. V. Priezjev, "Heterogeneous relaxation dynamics in amorphous materials under cyclic loading," Phys. Rev. E **87**, 052302 (2013).

[46] T. Kawasaki and L. Berthier, "Macroscopic yielding in jammed solids is accompanied by a nonequilibrium first-order transition in particle trajectories," Phys. Rev. E **94**, 022615 (2016).

[47] J. T. Uhl, S. Pathak, D. Schorlemmer, X. Liu, R. Swindeman, B. A. W. Brinkman, M. LeBlanc, G. Tsekenis, N. Friedman, R. Behringer, D. Denisov, P. Schall, X. Gu, W. J. Wright, T. Huf-

nagel, A. Jennings, J. R. Greer, P. K. Liaw, T. Becker, G. Dresen, and K. A. Dahmen, "Universal quake statistics: From compressed nanocrystals to earthquakes," Sci. Rep. **5**, 16493 (2015).

[48] N. P. Bailey, J. Schiøtz, A. Lemaître, and K. W. Jacobsen, "Avalanche size scaling in sheared three-dimensional amorphous solid," Phys. Rev. Lett. **98**, 095501 (2007).

[49] K. M. Salerno, C. E. Maloney, and M. O. Robbins, "Avalanches in strained amorphous solids: Does inertia destroy critical behavior?" Phys. Rev. Lett. **109**, 105703 (2012).

[50] P. Cao, K. A. Dahmen, A. Kushima, W. J. Wright, H. S. Park, M. P. Short, and S. Yip, "Nanomechanics of slip avalanches in amorphous plasticity," J. Mech. Phys. Solids **114**, 158–171 (2018).

[51] M.-C. Miguel, A. Vespignani, S. Zapperi, J. Weiss, and J.-R. Grasso, "Intermittent dislocation flow in viscoplastic deformation," Nature **410**, 667–671 (2001).

[52] D. M. Dimiduk, C. Woodward, R. LeSar, and M. D. Uchic, "Scale-free intermittent flow in crystal plasticity," Science **312**, 1188–1190 (2006).

[53] M. Zaiser, "Scale invariance in plastic flow of crystalline solids," Adv. Phys. **55**, 185–245 (2006).

[54] G. Wang, K.C. Chan, L. Xia, P. Yu, J. Shen, and W. H. Wang, "Self-organized intermittent plastic flow in bulk metallic glasses," Acta Mater. **57**, 6146 (2009).

[55] B. A. Sun, H. B. Yu, W. Jiao, H. Y. Bai, D. Q. Zhao, and W. H. Wang, "Plasticity of ductile metallic glasses: A self-organized critical state," Phys. Rev. Lett. **105**, 035501 (2010).

[56] J. Antonaglia, W. J. Wright, X. Gu, R. R. Byer, T. C. Hufnagel, M. LeBlanc, J. T. Uhl, and K. A. Dahmen, "Bulk metallic glasses deform via slip avalanches," Phys. Rev. Lett. **112**, 155501 (2014).

[57] K. A. Dahmen, Y. Ben-Zion, and J. T. Uhl, "A simple analytic theory for the statistics of avalanches in sheared granular materials," Nature Phys. **7**, 554–557 (2011).

[58] I. Regev, J. Weber, C. Reichhardt, K. A. Dahmen, and T. Lookman, "Reversibility and criticality in amorphous solids," Nature Comm. **6**, 8805 (2015).

[59] J. Brujić, S. F. Edwards, D. V. Grinev, I. Hopkinson, D. Brujić, and H. A. Makse, "3D bulk measurements of the force distribution in a compressed emulsion system," Faraday Discuss. **123**, 207–220 (2003).

[60] K. W. Desmond, P. J. Young, D. Chen, and E. R. Weeks, "Experimental study of forces between quasi-two-dimensional emulsion droplets near jamming," Soft Matter **9**, 3424–3436 (2013).

[61] R. Bandyopadhyay, D. Liang, H. Yardimci, D. A. Sessoms, M. A. Borthwick, S. G. J. Mochrie, J. L. Harden, and R. L. Leheny, "Evolution of particle-scale dynamics in an aging clay suspension," Phys. Rev. Lett. **93**, 228302 (2004).

[62] H. Guo, S. Ramakrishnan, J. L. Harden, and R. L. Leheny, "Connecting nanoscale motion and rheology of gel-forming colloidal suspensions," Phys. Rev. E **81**, 050401 (2010).

[63] Luca Cipelletti, S. Manley, R. C. Ball, and D. A. Weitz, "Universal aging features in the restructuring of fractal colloidal gels," Phys. Rev. Lett. **84**, 2275 (2000).

[64] J.-P. Bouchaud and E. Pitard, "Anomalous dynamic light scattering in soft glassy gels," Eur. Phys. J. E **6**, 231–236 (2001).

[65] L. Cipelletti, L. Ramos, S. Manley, E. Pitard, D. A. Weitz, E. E. Pashkovski, and M. Johansson, "Universal non-diffusive slow dynamics in aging soft matter," Faraday Discuss. **123**, 237–251 (2003).

[66] D. Fiocco, G. Foffi, and S. Sastry, "Encoding of memory in sheared amorphous solids," Phys. Rev. Lett. **112**, 025702 (2014).

[67] N. C. Keim and P. E. Arratia, "Yielding and microstructure in a 2D jammed material under shear deformation," Soft Matter **9**, 6222–6225 (2013).

[68] K. Hima Nagamanasa, S. Gokhale, A. K. Sood, and R. Ganapathy, "Experimental signatures of a nonequilibrium phase transition governing the yielding of a soft glass," Phys. Rev. E **89**, 062308 (2014).